Title

Myeloid DAP12-associating lectin (MDL)-1 regulates synovial inflammation and bone erosion associated with autoimmune arthritis.

Journal

The Journal of experimental medicine, 207(3)

ISSN

0022-1007

Authors

Joyce-Shaikh, Barbara
Bigler, Michael E
Chao, Cheng-Chi
et al.

Publication Date

2010-03-01

DOI

10.1084/jem.20090516

Peer reviewed

Myeloid DAP12-associating lectin (MDL)-1 regulates synovial inflammation and bone erosion associated with autoimmune arthritis

Barbara Joyce-Shaikh, Michael E. Bigler, Cheng-Chi Chao, Erin E. Murphy, Wendy M. Blumenschein, Iannis E. Adamopoulos, Paul G. Heyworth, Svetlana Antonenko, Edward P. Bowman, Terrill K. McClanahan, Joseph H. Phillips, and Daniel J. Cua

Department of Discovery Research, Schering-Plough Biopharma, Palo Alto, CA 94304

DNAX adaptor protein 12 (DAP12) is a trans-membrane adaptor molecule that transduces activating signals in NK and myeloid cells. Absence of functional *Dap12* results in osteoclast defects and bone abnormalities. Because DAP12 has no extracelluar binding domains, it must pair with cell surface receptors for signal transduction. There are at least 15 known DAP12-associating cell surface receptors with distinct temporal and cell type–specific expression patterns. Our aim was to determine which receptors may be important in DAP12-associated bone pathologies. Here, we identify myeloid DAP12-associating lectin (MDL)-1 receptor (also known as CLEC5A) as a key regulator of synovial injury and bone erosion during autoimmune joint inflammation. Activation of MDL-1 leads to enhanced recruitment of inflammatory macrophages and neutrophils to the joint and promotes bone erosion. Functional blockade of MDL-1 receptor via *Mdl1* deletion or treatment with MDL-1-Ig fusion protein reduces the clinical signs of autoimmune joint inflammation. These findings suggest that MDL-1 receptor may be a therapeutic target for treatment of immune-mediated skeletal disorders.

CORRESPONDENCE
Daniel J. Cua:
daniel.cua@spcorp.com

Abbreviations used: CAIA, collagen antibody-induced arthritis; CIA, collagen-induced arthritis; DAP12, DNAX adaptor protein 12; HRP, horseradish peroxidase; ITAM, immunoreceptor tyrosine-based activation motif; MCSF, macrophage colony-stimulating factor; MDL, myeloid DAP12-associating lectin; RA, rheumatoid arthritis; RANKL, receptor activator of NF-κB ligand.

The balance between osteoblast and osteoclast activation and function is critical for bone homeostasis. Osteoblasts, which are cells of mesenchymal origin, secrete bone-matrix proteins to promote mineralization; whereas macrophages, neutrophils, and osteoclasts, which are derived from a common hematopoietic precursor, are key contributors to the pathogenesis in bone resorptive disorders such as rheumatoid arthritis (RA). During autoimmune joint disease the excessive influx of inflammatory macrophages and granulocytes leads to an increased development and activation of osteoclasts. The inflammatory response promotes tissue injury and osteoclast activation, which leads to detrimental cartilage and bone loss. The primary signals for this process are induced in the presence of M-CSF by receptor activator of NF-κB ligand (RANKL), which in turn activates the TRAF6, c-Fos, and the NFATc1 pathway (Ishida et al., 2002; Takayanagi, 2002, 2005a). Additional co-stimulatory signals derived from immunoreceptor tyrosine-based activation motif (ITAM)–containing molecules are also essential for osteoclastogenesis (Koga et al., 2004). DNAX adaptor protein 12 (DAP12) is a trans-membrane adaptor molecule that transduces activating signals via ITAM for a range of cell surface receptors on NK cells, granulocytes, and macrophages (Lanier et al., 1998; Kaifu et al., 2003). There are many known DAP12 pairing partners, including myeloid DAP12-associating lectin-1 (MDL-1), which has been shown to regulate myeloid cell–associated inflammatory responses (Bakker et al., 1999; Aoki et al., 2004; Chen et al., 2008). MDL-1—a C-type lectin domain family 5, member A (CLEC5A)—is highly expressed on TNF-activated macrophages (Bakker et al., 1999). Cross-linking cell surface MDL-1 receptors induces DAP12-ITAM–dependent calcium mobilization (Bakker et al., 1999) and activation of the Syk and

The Rockefeller University Press $30.00
J. Exp. Med. Vol. 207 No. 3 579-589
www.jem.org/cgi/doi/10.1084/jem.20090516

The Journal of Experimental Medicine

phospholipase Cγ signaling pathways (Lanier et al., 1998; Mao et al., 2006). The ITAM-dependent calcium signaling pathway is a critical "co-stimulatory" signal for RANKL-dependent regulation of bone remodeling and homeostasis (Takayanagi, 2005a).

Although MDL-1 expression is up-regulated in activated myeloid cells, it is not known whether this receptor plays any role in autoimmune inflammation. Given the fact that MDL-1's pairing partner, DAP12, has a role in osteoclast formation and bone remodeling (Humphrey et al., 2004, 2006; Kaifu et al., 2003), we tested whether MDL-1 activation could affect autoimmune arthritis. In this study, we demonstrate that MDL-1 is expressed on inflammatory macrophages and neutrophils, as well as bone marrow–derived osteoclast precursors. Activation of the MDL-1 receptor during joint inflammation enhances myeloid cell infiltration and promotes IL-1, IL-6, IL-17A, and TNF expression, resulting in severe cartilage damage and bone erosion. In contrast, neutralization of MDL-1 function down-regulates TRAP, cathepsin K, and MMP9 expression, subsequently preserving bone mineral density. These results suggest that therapeutic targeting of the MDL-1 receptor may suppress inflammation and, ultimately, bone resorptive pathways during inflammatory conditions.

RESULTS

MDL-1 receptor is expressed on bone marrow cells and inflamed joints

In a tissue array gene expression analysis of MDL-1 receptor, we found that human (Fig. 1 A) and mouse (Fig. 1 B) bone marrow cells and joint tissues express the highest levels of *Mdl1*. Correspondingly, MDL-1 protein is expressed on murine granulocytes ($CD11b^+$ $Ly6G^+$) and monocytes ($CD11b^+$ $Ly6G^-$) from bone marrow and the peripheral blood (Fig. 1 C). We observed that activation with TNF, but not IFN-γ, further enhances *Mdl1* mRNA and protein expression in bone marrow–derived macrophage colony-stimulating factor (MCSF)-dependent macrophages (Fig. 1 D). To assess whether triggering the MDL-1 receptor could activate myeloid cells, we generated mAbs that are capable of cross-linking and promoting MDL-1 activation. To test the antibody specificity and function, we performed a bioassay where cellular degranulation can be triggered by MDL-1/DAP12 phosphorylation (see Materials and methods). Treatment of an MDL-1/DAP12-transfected mast cell line with an anti–MDL-1 mAb (clone DX163) induces specific degranulation, demonstrating that clone DX163 is an agonistic mAb that activates the MDL-1–DAP12 signaling pathway (Fig. S1). We next confirmed the activities of the anti–MDL-1 mAb in primary cells. Wild-type, but not *Dap12*$^{-/-}$, macrophages produced inflammatory mediators in response to anti–MDL-1 treatment. TNF, G-CSF, IL-1β, and MCP-1 (Fig. 1 E and not depicted) were up-regulated by anti–MDL-1 antibodies, and this was further enhanced in the presence of LPS, a TLR-4 agonist.

MDL-1 receptor activation enhances inflammatory cell infiltration, cartilage damage, and bone erosion

The *Mdl1* mRNA expression in bone marrow and synovium prompted us to determine which cell types might express this immune regulator in human RA tissue. We found that MDL-1 is highly expressed on myeloid cells in the inflamed pannus. We also observed the same expression pattern in mouse inflamed joint (not depicted). The expression of MDL-1 appears to colocalize with a subset of $CD68^+$ inflammatory macrophages, as indicated by the immunostaining of serial sections from synovial RA samples (Fig. S2). To confirm colocalization of MDL-1 with myeloid cells in inflamed pannus, we performed immunofluorescent staining with anti–MDL-1 (phycoerythrin) and CD11b (FITC). Interestingly, most, but not all, of the $CD11b^+$ cells also coexpress MDL-1 as shown in the merged immunofluorescent images, which appeared yellow (Fig. S2).

Given the expression pattern of MDL-1 in joint tissues, we examined its expression on leukocytes during a collagen antibody-induced arthritis (CAIA) model. This disease is induced by passive transfer of type II collagen-specific antibodies and requires direct myeloid cell activation to promote pathology. We found that $CD11b^+$ $Ly6G^+$ MDL-1^+ cells increased from 35 to 50% in the bone marrow 7 d after arthritis induction. Similarly, MDL-1^+ cells in peripheral blood increased from 25% in controls to 40% in arthritic mice (Fig. S3). We next determined the function of MDL-1 in CAIA using anti–MDL-1 agonist mAbs that specifically cross-link and activate the MDL-1 receptor pathway. Mice given anti–MDL-1 agonists in conjunction with the arthrogenic antibody cocktail exhibit increased disease incidence and severity (Fig. 2 A). Anti–MDL-1 treatment promoted an increase in the total number of bone marrow $CD11b^+$ $Ly6G^+$ granulocytes and $CD11b^+$ $Ly6G^-$ monocytes compared with isotype-treated controls (Fig. 2 B). This increase correlated with higher levels of total MPO activity in the bone marrow (not depicted) and elevated circulating peroxidase-positive (%HPX) neutrophils and monocytes (Fig. 2 C and not depicted), indicating that activation of MDL-1 promoted expansion of "reactive" myeloid cells capable of inducing tissue damage. As early as 1 d after disease onset, anti–MDL-1 agonist-treated mice already showed greater clinical scores compared with the isotype control group. By day 4, histopathology shows a dramatic increase in neutrophil infiltration into the arthritic paws of anti–MDL-1–treated mice (>60% PMNs) compared with isotype-treated controls (20% PMNs), which corresponds with intense cartilage damage, bone erosion, and pannus tissue formation (Fig. 2, D and E). By day 11, the extent of damage in the anti–MDL-1 treatment group is remarkable, with near maximum pathology scores for inflammatory cell infiltrate, articular cartilage destruction, and almost complete cortical bone erosion of the metatarsalphalange joints. To assess the roles of granulocytes/monocytes in this MDL-1–driven disease, mice were given anti-GR1 mAb, which depletes $Ly6G^+$ granulocytes and a subset of $Ly6G^+/Ly6C^+$ monocytes. In vivo depletion was confirmed

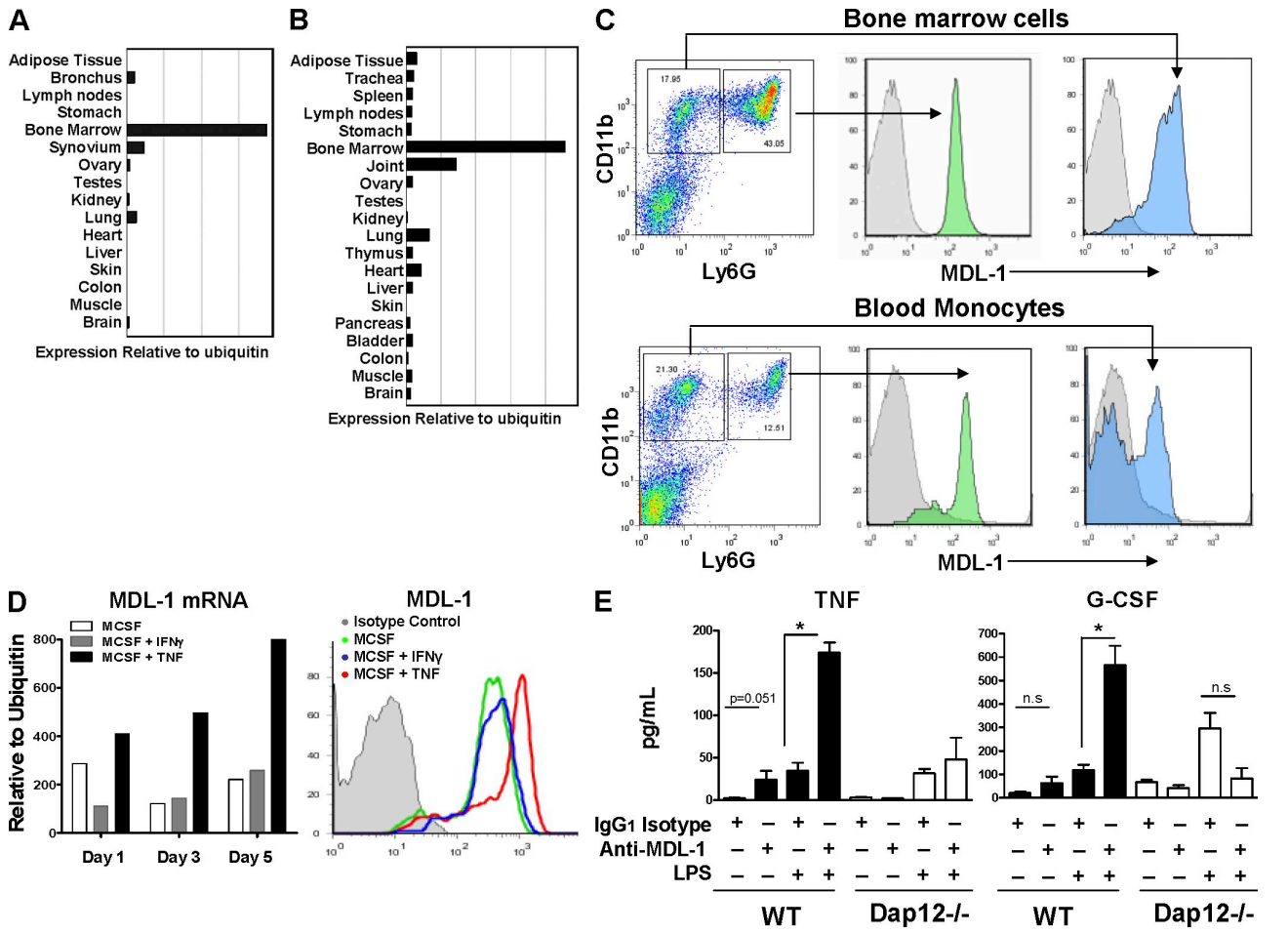

Figure 1. Regulation of MDL-1 receptor expression. (A and B) Bone marrow cells and joint tissues show the highest level of MDL-1 expression. Quantitative PCR analysis of human (A) and mouse (B) anatomy panels generated from pooled tissue samples from at least five donors. (C) MDL-1 is expressed on murine granulocytes (CD11b + Ly6G high) and monocytes (CD11b + Ly6G low) from bone marrow and peripheral blood. Histograms in gray color are rIgG2a isotype staining controls. Data are representative of three experiments. (D) TNF but not IFN-γ promotes MDL-1 expression. Murine bone marrow cells were cultured with MCSF in the presence of IFN-γ or TNF and mRNA was isolated for MDL-1 expression analysis by Q-PCR. Cell surface expression of MDL-1 was determined by flow cytometry. Data representative of at least three separate experiments with similar results. (E) Anti–MDL-1 activates bone marrow–derived macrophages to produce TNF and G-CSF. Bone marrow cells isolated from three mice were cultured with indicated antibodies and/or LPS for 36 h. Culture supernatants were assayed for secreted cytokines by Luminex assay. * indicates significance ($P < 0.01$) as determined by Student's *t* test. Results are representative of three separate experiments with similar results.

by flow cytometry shown in Fig. S4. Mice given anti-GR1 treatment 1 d before induction of MDL-1–driven CAIA showed significant disease amelioration, indicating that GR1-positive myeloid cells play an important role in promoting MDL-1–activated joint inflammation (Fig. 2 F).

We also assessed the role of MDL-1 receptor in collagen-induced arthritis (CIA), which is a T, B, and myeloid cell–dependent model of arthritis. Mice were immunized with type II collagen and treated with anti–MDL-1 agonist mAb on the day of clinical disease onset (day 18 after collagen immunization). 2 d after MDL-1 activation, we already noticed enhanced joint swelling response. The disease quickly progressed to a very severe form of arthritis (Fig. S5). These results prompted us to investigate whether specific blockade of MDL-1 could inhibit inflammatory joint disease.

Absence of MDL-1 receptor inhibits joint inflammation and preserves bone density

Based on the association of DAP12 and MDL-1 with joint diseases, we determined if blockade of this innate inflammatory pathway could attenuate myeloid cell–mediated joint inflammation and bone erosion. Mice were generated in which all six exons of *Mdl1* were deleted via homologous recombination using C57BL/6 embryonic stem cells (Fig. S6). Successful deletion of *Mdl1* was confirmed by PCR and flow cytometry. $Mdl1^{-/-}$ mice are viable and born in the expected Mendelian ratios. The number of myeloid and lymphoid cell subsets is similar in $Mdl1^{-/-}$ and wild-type mice (unpublished data). CAIA disease incidence and severity of both $Dap12^{-/-}$ and $Mdl1^{-/-}$ are reduced compared with wild-type mice (Fig. 3 A). In addition, analysis of proinflammatory cytokines

and osteoclast markers in arthritic paws show a protective effect of deleting *Mdl1* and *Dap12* (Fig. 3 B). The absolute values of these inflammatory genes in arthritic and naive control paws are shown in Fig. S7.

Because the endogenous ligand for the MDL-1 receptor has not been identified, we generated a soluble MDL-1 molecule, which would be expected to engage the ligand and inhibit the in vivo activities of MDL-1. This soluble MDL-1 antagonist is composed of a murine FcγRI binding-deficient mutant IgG2a covalently linked to the extracellular portion of MDL-1 (MDL-1–Ig fusion protein). MDL-1–Ig fusion–treated mice were highly resistant to both CIA and CAIA compared with controls (Fig. 3, C and D). In the CIA study, the MDL-1–Ig-fusion treatment was initiated at day 18 when

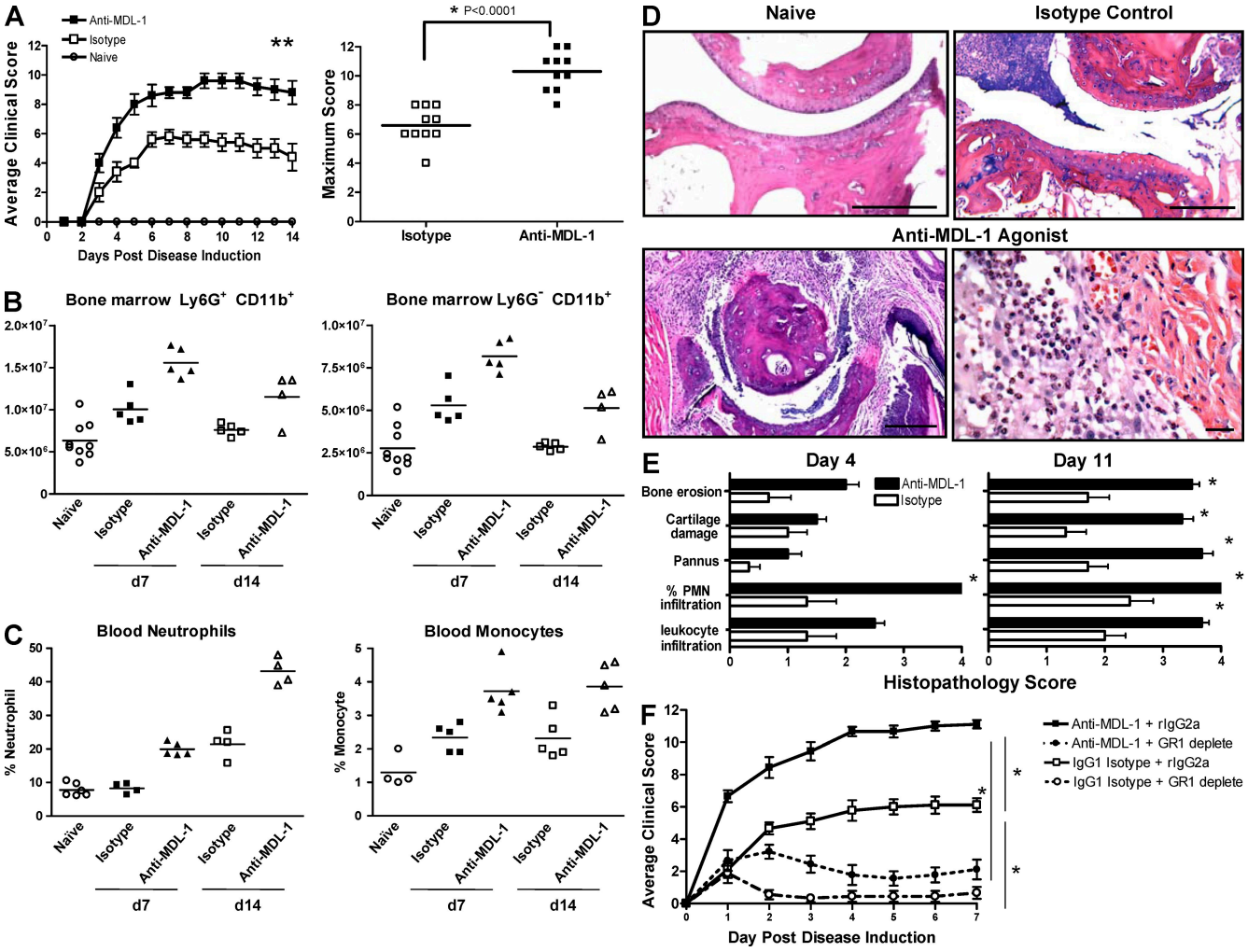

Figure 2. MDL-1 activation enhances autoimmune arthritis. (A) Treatment with anti–MDL-1 agonist mAb exacerbates CAIA. B10RIII mice (n = 5/group) were given arthrogen to induce arthritis. Mice treated with anti–MDL-1 mAb (clone DX163) at the time of arthrogen treatment showed disease exacerbation compared with isotype controls. Maximum clinical score of individual mice from two separate anti–MDL-1 treatment studies is shown on the right. Results are representative of at least four experiments. (B) Anti–MDL-1 treatment increases the absolute number of bone marrow granulocytes and monocytes. Each data point is FACS analysis of cells extracted from two tibias. (C) Peripheral blood peroxidase-positive neutrophils and macrophages are elevated in anti–MDL-1 treated mice, as shown by ADVIA analysis. The studies in B and C were performed twice. (D) Representative H&E-stained micrographs of metatarsal-phalange joints from the study shown in A. Bars: (top left, bottom left, and top right) 200 µm; (bottom right) 60 µm. The anti–MDL-1 agonist treatment group showed intense neutrophil and macrophage infiltration, as well as pannus tissue formation with extensive bone erosion. (E) Histopathology was performed in a masked fashion. Leukocyte infiltration and percentage of PMN infiltration were determined in the synovium and joint space. Percent PMNs: 1 = <20%, 2 = 20–40%, 3 = 40–60%, and 4 = >60%. Pannus tissue formation, cartilage destruction, and cortical bone erosions were assessed as described in the Materials and methods section. The severity was graded on a scale of 0–4. Comparisons between anti–MDL-1 and isotype control were determined using the Mann Whitney U test. * indicates $P < 0.05$ and is considered statistically significant. (F) Depletion of granulocytes/monocytes reduced anti–MDL-1–driven CAIA. Date shown are summary of two separate experiments (n = 10 per treatment group). Disease was induced as in A with additional groups that were pretreated on day −1 with anti-GR1 mAb (clone RB6-8C5, rIgG2a isotype) that depletes Ly6G$^+$ and a subset of Ly6C$^+$ cells. Disease was induced on day 0 and mice were given anti–MDL-1 mAb (clone DX163) or an IgG1 isotype control. Depletion of GR1$^+$ populations was confirmed by flow cytometry (Fig. S4).

~40% of the mice ($n = 29$ from 2 studies) already showed initial clinical signs of disease. Strikingly, only a few days after MDL-1–Ig treatment, the arthritic mice already demonstrated clinical improvement. This contrasts with the rapid disease progression observed in isotype controls and anti–MDL-1 agonist–treated mice (Fig. 3 C). In CAIA studies, MDL-1–Ig treatment also displays similar protection from disease (Fig. 3 D). Histopathological assessment of hind paws showed the isotype control group have mild cellular infiltrate and bone erosion, whereas mice treated with the MDL-1–Ig fusion protein have little or no pathological signs of disease (Fig. S8).

We confirmed the histopathology findings and quantified the magnitude of bone destruction using x-ray microCT analysis. The bone mineral density and the bone structural changes of articular phalangeal joints were assessed at day 11 after CAIA induction. Fig. 4 A shows high resolution three dimensional rendering of microCT scans of hind paws. Anti–MDL-1 agonist treatment induces considerable cortical bone destruction, whereas MDL-1–Ig fusion protein—which functions as an effective antagonist—dramatically blocks bone erosion. Although histopathology findings show intense cortical bone erosion at the joint space of anti–MDL-1–treated

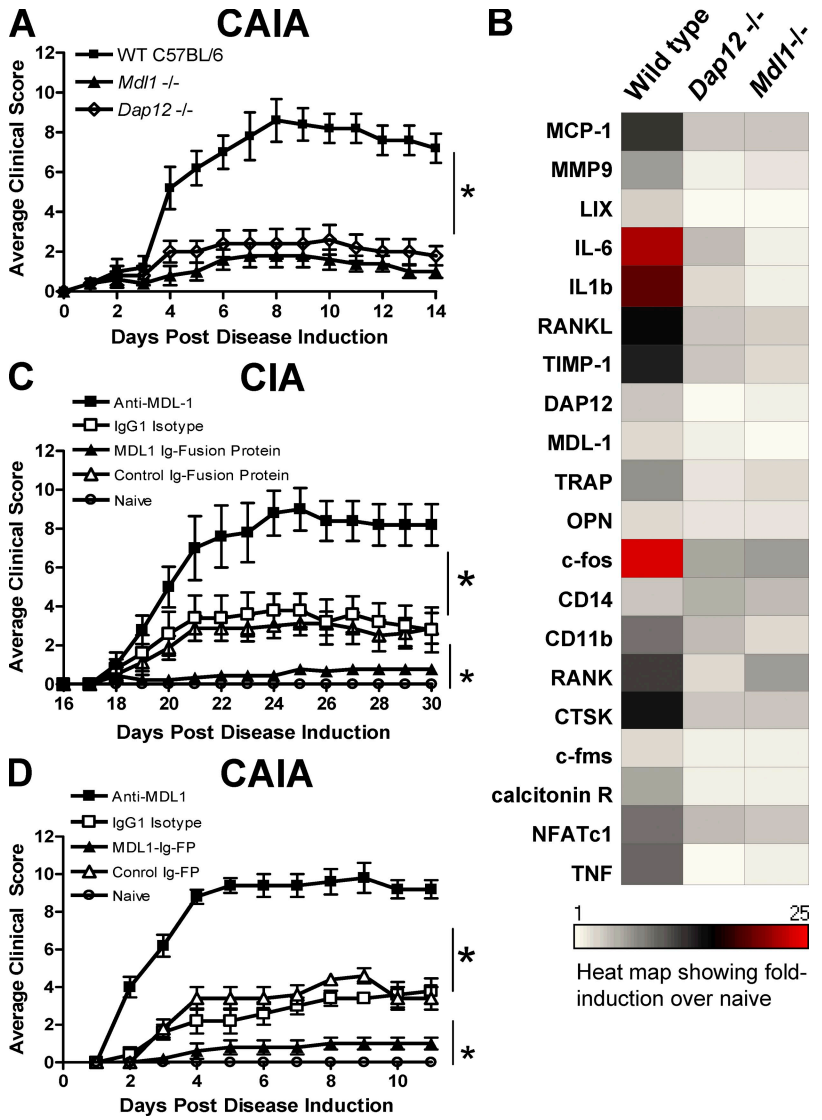

Figure 3. MDL-1 blockade inhibits autoimmune arthritis. (A) C57BL/6 control, *Dap12*$^{-/-}$, and *Mdl1*$^{-/-}$ mice were injected with arthrogenic mAbs to induce CAIA. Mean clinical scores ($n = 5$/group) ± SEM are shown. Result is representative of two studies. * indicates statistical significance. (B) Hind paw mRNA from A was isolated for gene expression analysis. The absolute values of the inflammatory genes are shown in Fig. S7. (C) MDL-1 activation enhanced T cell– and myeloid cell–dependent arthritis. B10RIII mice were immunized with bovine type II collagen emulsified in CFA at day 0 to induce collagen-induced arthritis. Anti–MDL-1 agonist (clone DX163) was given on day 18 of immunization. Statistical significance was determined by analysis of variance (ANOVA). Results are representative of two studies. (D) B10RIII mice ($n > 5$/group) were given 1.5 mg of Arthrogen to induce CAIA. MDL-1 Ig fusion protein or control proteins were administrated at the time of Arthrogen treatment. * indicates statistical significance ($P < 0.001$) as determined by ANOVA analysis.

mice, the microCT three dimensional image reconstruction produced images suggestive of metaphyseal damage. This may be because if the rendering of a three dimensional dataset into a two dimensional picture and is consistent with previously published MicroCT results in mouse arthritis models (Barck et al., 2004). To quantify the extent of the bone destruction, we performed histomorphometric analysis of cortical bones and determined that MDL-1 agonist mAb-treated mice show substantial loss of bone volume, bone density, and cortical thickness compared with the moderate changes in the Ig control groups (Fig. 4 B). In contrast, MDL-1–Ig fusion–treated mice have bone integrity, density, volume, and bone mass values that are nearly comparable to healthy naive mice, confirming that blocking MDL-1 receptor activation maintains joint integrity. It has been shown that circulating levels of TRAP 5b are proportional to the number of osteoclasts (Scarnecchia et al., 1991; Henriksen et al., 2007). By testing serum samples during the course of disease, we found that the osteoclast-specific TRAP 5b levels were significantly increased after MDL-1 receptor activation (Fig. 4 C). The elevated TRAP 5b levels correlate with the enhanced bone erosion in the anti–MDL-1–treated mice. RANKL levels are also increased in anti–MDL-1 agonist–treated mice, whereas MDL-1-Ig fusion–treated mice have levels comparable to naive animals.

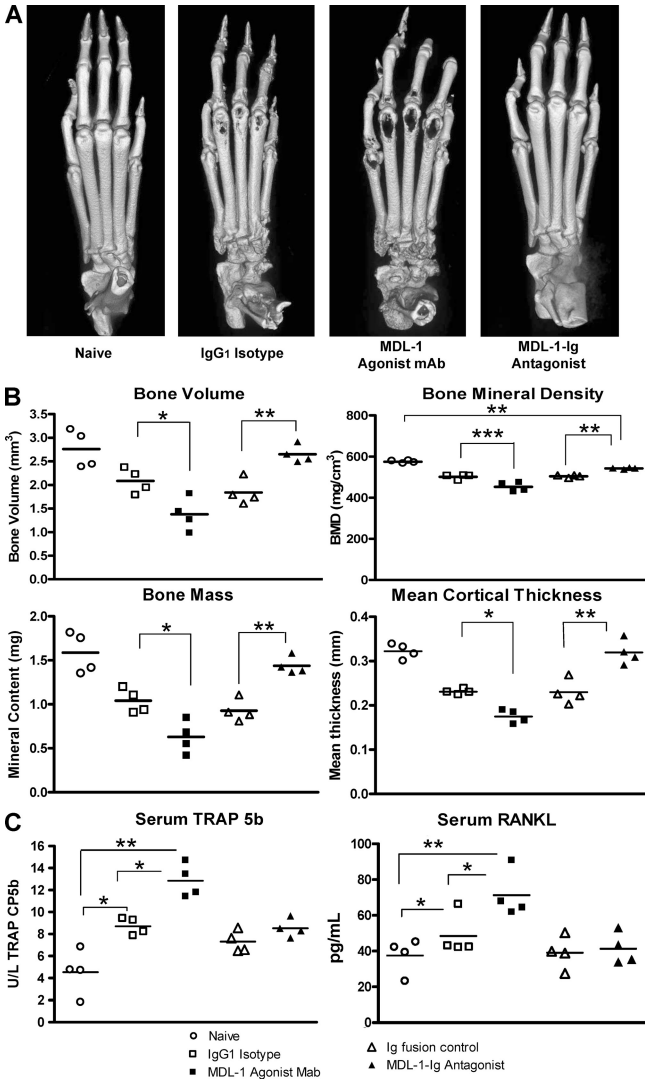

Figure 4. MDL-1 blockade inhibits bone erosion and inflammation. (A) Hind paws from mice in Fig. 3D were harvested on day 11 and prepared for MicroCT analysis. Images show high resolution three-dimensional rendering of MicroCT scans. MDL-1 Ig-fusion protein (antagonist)–treated mice show no sign of cortical bone destruction, whereas the agonist MDL-1 antibody (clone: DX163) treated mice show greater bone destruction than control IgG1-treated mice. Results are representative of three separate experiments. (B) Quantification of bone integrity indicates increased bone loss in anti–MDL-1 agonist-treated mice. Comparable regions of interest (ROI) consisting of three metatarsal joints from each mouse were selected for analysis. Bone volume (BV), bone mass (BM), bone mineral density (BMD = BM/BV mg/cm^3), and mean cortical thickness (mm) were quantified from MicroCT scans using GE MicroView software v2.2. Student's *t* test was used to determine significance where ***, $P < 0.001$; **, $P < 0.01$; *, $P < 0.05$. (C) ELISA quantification of Serum TRAP 5b and RANKL. Day 20 serum levels of TRAP5b and RANKL from individual mice are shown. TRAP5b levels from day 11 also show similar results. * indicates $P < 0.05$ by Student's *t* test analysis.

MDL-1 signaling regulates osteoclast function

To investigate the immune responses regulated by MDL-1 activation, we assessed the expression of proinflammatory cytokines, osteoclast markers, and myeloid cell markers in arthritic paws. On day 4 after induction of CAIA, which is just before the peak of paw swelling response in the control groups, proinflammatory genes including IL-1β, IL-6, and IL-17 are suppressed in MDL-1–Ig fusion protein–treated mice, whereas the anti–MDL-1–treated group show enhanced cytokine gene expression (Fig. 5 A). Importantly, genes associated with bone destruction such as RANKL, MMP9, ATPV0D2, and TRAP are down-regulated in paws after MDL-1–Ig fusion treatment and up-regulated in anti–MDL-1 agonist treatment. Also, myeloid cell–specific genes including CD11b, RANK, and DAP12 are reduced in the MDL-1–Ig fusion group and elevated in anti–MDL-1 agonist group. In addition, CXCL1, which promotes neutrophil recruitment, is also up-regulated by the MDL-1 agonist. We also determined the gene expression of arthritic paws at day 11 and found similar patterns (unpublished data). Interestingly, even through MDL-1 activation enhanced TNF, IL-6, RANK, and TRAP expression, both type I and II IFNs were undetectable in the inflamed paws (the Q-PCR cycle threshold is ~40), consistent with the concept that MDL-1 is linked with the TNF–RANKL pathway rather than the IFN–STAT1 pathway that inhibits bone resorption mechanisms.

The apparent regulation of the TRAP, RANKL, ATPV0D2, and MMP9 expression after anti–MDL-1 treatment suggests MDL-1 receptor activation may promote osteoclast development and function. To test this, we treated wild-type bone marrow cells with an anti–MDL-1 agonist in the presence of RANKL (10 ng/ml). MDL-1 activation increases the kinetics of cell fusion, resulting in greater size and frequency

of mature osteoclasts (Fig. 5 B). These results suggest MDL-1 activation promotes in vitro osteoclastogenesis and cell fusion. TRAP and cathepsin K are osteoclast-specific genes regulated by the NFATc1 transcription factor (Matsumoto et al., 2004; Takayanagi, 2005a). To determine whether MDL-1 directly regulates NFATc1, anti–MDL-1–activated bone marrow cells were prepared for NFATc1 nuclear lysate ELISA. MDL-1 + RANKL induced a significant increase of phospho-NFATc1 nuclear localization over RANKL alone, indicating that MDL-1-DAP12–mediated signaling promotes amplification of this transcription regulator required for osteoclast differentiation (Fig. 5 C). These in vitro osteoclast

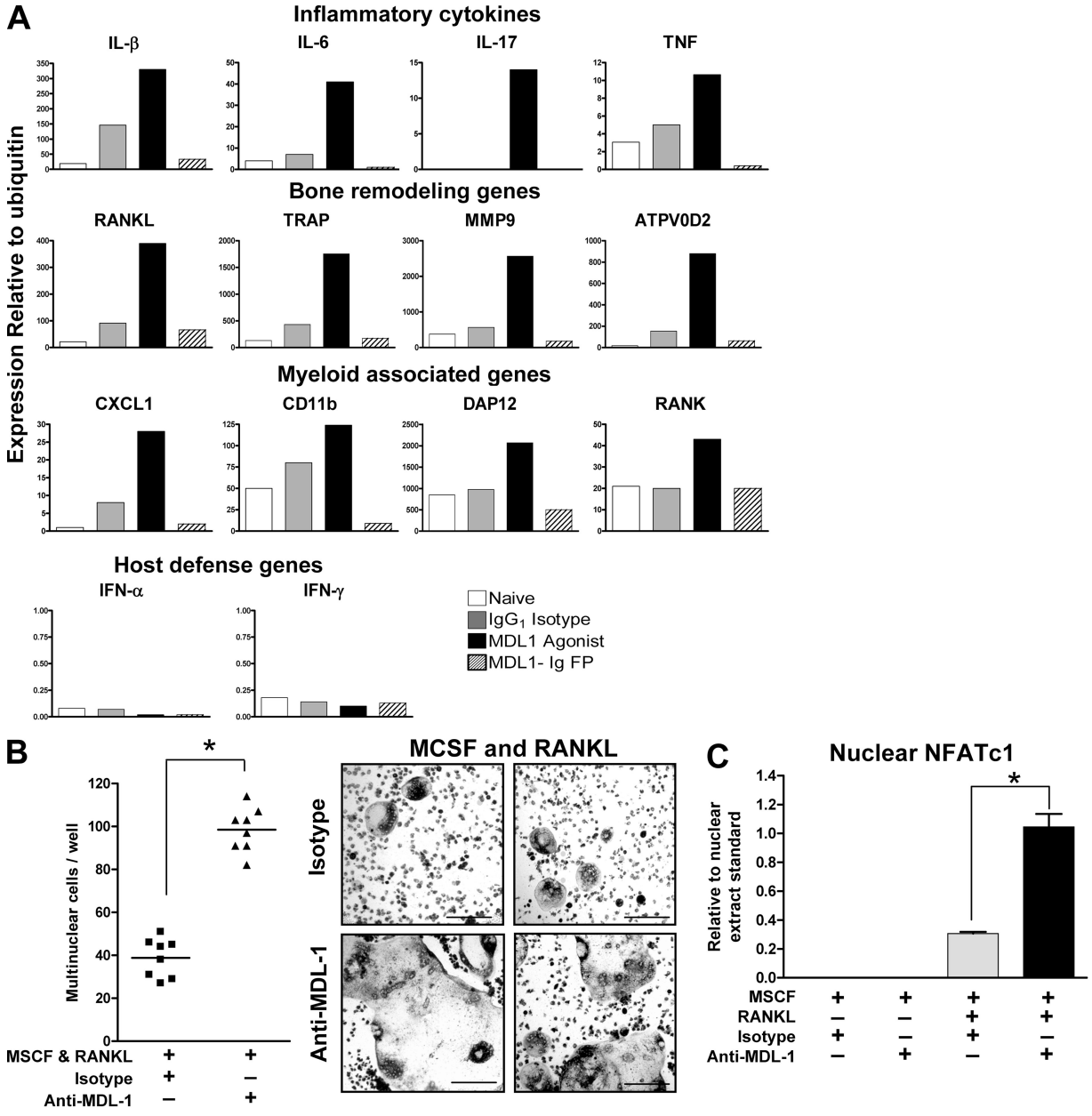

Figure 5. MDL-1 activation promotes NFATc1 nuclear translocation and enhances osteoclast formation. (A) Gene expression of pooled (n = 3) hind paws treated as in Fig. 3D were harvested at day 4 and prepared for Q-PCR analysis. Data are representative of four experiments. (B) Bone marrow cells were cultured in plastic dishes in the presence of 10 ng/ml RANKL and MCSF. Anti–MDL-1, but not isotype control (or medium control; not depicted) increased the number multinuclear cells (left) and osteoclast size (right). Data are representative of at least four separate experiments. Bars, 200 µm. (C) MDL-1 regulates NFATc1 nuclear expression. C57BL/6 bone marrow cells were cultured with indicated growth factors and antibodies. Cells were cultured for 6 d and nuclear lysates prepared for Active Motif Nuclear NFATc1 colorimetric assay. Nuclear NFATc1 was detected by a plate-bound NFAT oligonucleotide consensus sequence (5′-AGGAAA-3′), a primary NFATc1-specific antibody, and a secondary HRP-conjugated mAb. Results are representative of two studies. * indicates significance ($P < 0.01$) as determine by ANOVA analysis.

functional assays, together with our in vivo observations that blockade of MDL-1 function reduces autoimmune joint inflammation and bone erosion, suggest that MDL-1 plays a critical role in joint diseases.

DISCUSSION

In this study, we have identified MDL-1 receptor as a key mediator of autoimmune joint inflammation. It appears that MDL-1 activation contributes to two distinct cellular mechanisms of tissue destruction. Not only does MDL-1 activation recruit substantial numbers of bone marrow–derived inflammatory macrophages and neutrophils, it also promotes osteoclast activation. Depletion of circulating granulocytes and/or monocytes significantly reduces MDL-1–dependent joint inflammation during CAIA, suggesting that inflammatory macrophages and neutrophils play a key role in MDL-1–mediated pathology. Direct Blockade of MDL-1 function also down-regulates paw swelling responses and inhibits pannus tissue formation while preserving bone volume and mineral density. We also demonstrate that MDL-1 activation increases the expression of NFATc1 and ATPV0D2, which control cell fusion (Lee et al., 2006), as well as regulating bone resorption via TRAP and cathepsin K in osteoclasts (Takayanagi, 2005a). These results suggest that targeting the MDL-1 pathway may modulate several important biological processes that control bone metabolism and inflammatory bone disease.

Previous studies have shown that the pairing partner of MDL-1 receptor—DAP12 has important roles in bone metabolism. Patients with loss of function mutations in DAP12 present with polycystic lipomembranous osteodysplasia and sclerosing leukoencephalopathy, also known as Nasu-Hakola disease. In a linkage disequilibrium analysis, Paloneva et al. (2000) mapped this disease to a 1.8-Mb region of chromosome 19Q13.1. Sequencing the candidate genes in this region revealed *Dap12* to carry several disease-associated variants, including a homozygous deletion encompassing exons 1–4. Nasu-Hakola disease is characterized by lipid-filled bone cysts found in articular joints of young adult patients, which leads to bone pain and fractures (Mii et al., 1991). These patients also show signs of presenile dementia associated with loss of myelin in the frontal lobe in addition to the osteoporotic features. However, peripheral blood mononuclear cells from the *Dap12*-deficient patients exhibit a delayed differentiation of osteoclasts with reduced bone resorption capability (Paloneva et al., 2003). The reduced in vitro osteoclast activity does not match the decreased trabecular bone density in *Dap12*-deficient patients (Paloneva et al., 2001). In preliminary trabecular bone measurement studies, we found differences between $Dap12^{-/-}$ and $Mdl1^{-/-}$ mice. Consistent with previous studies (Humphrey et al., 2004, 2006), $Dap12^{-/-}$ mice show mild osteopetrosis. Unexpectedly, $Mdl1^{-/-}$ mice show a dysregulated bone phenotype with irregular trabecular bone connectivity (unpublished data). Future studies are needed to address the relative contribution of MDL-1 and DAP12 in bone homeostasis.

Although the endogenous ligands for the MDL-1 receptor have not been identified, a recent study has demonstrated that the dengue virus capsid protein activates the MDL-1–DAP12–ITAM pathways leading to intense immune pathologies during the viral infection (Chen et al., 2008). The hallmarks of dengue "break-bone" fever are cytokine storm, vascular leakage, and severe joint pain (Mathew and Rothman, 2008). Intriguingly, in a mouse model of dengue hemorrhagic disease, specific blockade of MDL-1 receptor inhibited the cytokine storm and vascular leakage. This tissue damage is associated with excessive IL-6, TNF, and MIP-1a production without affecting IFN-α production (Chen et al., 2008). This is consistent with our observation that MDL-1 activation induced TNF, IL-1β, IL-6, (which is linked with NF-κB, TRAF6, and STAT3 activation) but not IFN-α and IFN-γ (STAT1 activation). Resent studies have shown that both type I and II IFNs have profound STAT1-dependent inhibitory effects on immune-mediated arthritis and osteoclast formation (Takayanagi et al., 2005b). This is consistent with our observation that MDL-1 expression on myeloid cells is enhanced by TNF but not IFN-γ (Fig. 1).

A recent study has uncovered the molecular basis for TNF-dependent bone resorption versus tissue inflammation (Ochi et al., 2007). TNF was shown to promote bone loss by inducing osteoclast expression of paired Ig-like receptor A (PIR-A), which partners and signals via ITAM-containing Fc receptor γ (FcRγ). This induced accelerated osteoclastogenesis, which correlated with enhanced bone destruction and osteoporosis. Interestingly, when the PIR-A–FcRγ pathway was inhibited, TNF still promoted soft tissue inflammation, but not bone resorption. In this study, we show that blocking MDL-1–DAP12 predominantly reduced tissue inflammation by reducing TNF, IL-1β, and IL-6 secretion and neutrophil/macrophage infiltration. Further studies are required to confirm the MDL-1–intrinsic role of osteoclast development and bone resorptive function.

It is increasingly evident that merely targeting inflammation alone may not be an adequate treatment for many types of joint disorders because bone resorption is an integral part of these diseases. Therefore, new therapeutic strategies need to incorporate both antiinflammatory and antiresorptive activities. The possibility that MDL-1 may regulate both inflammatory and bone resorptive mechanisms makes this a promising target for treatment of inflammatory arthritis. We have bridged the findings in our mouse studies to human diseases by demonstrating human MDL-1 expression in synovial tissues from RA patients. Further clinical studies are needed to confirm a pathogenic role for MDL-1 in human skeletal disorders and to determine whether this DAP12-paring receptor is a therapeutic target for treatment of inflammatory and/or degenerative bone disorders.

MATERIALS AND METHODS

Reagents and antibodies. MDL-1 (GenBank/EMBL/DDBJ accession no. BC112099). Anti–mMDL-1 agonist (clone: DX163) was generated from rats using immunogenic fusion proteins consisting of the extracellular domain of the mouse MDL-1 gene, including the amino acid positions 26–166 (GenBank/EMBL/DDBJ accession no. AF139769). Both anti–MDL-1 mAbs are IgG1 isotype. Mouse MDL-1 fusion protein was generated as follows: extracellular (163 amino acids) portion of mouse MDL-1 (GenBank/EMBL/DDBJ accession no. AA186015) was ligated into a pCMV1 expression plasmid containing the Fc portion of mIgG2a that has been mutated (L to E) for low FcγRI binding properties. Protein was expressed in 293 freestyle cells.

Acquisition of human tissue. Human synovial samples were obtained under informed consent from RA patients under a protocol approved by the Stanford University IRB and performed at the Stanford University Hospital. For the human anatomy panel, depending on the collection protocols established at each site, tissues were acquired either under IRB-approved waiver of consent (NDRI and CHTN) or by informed consent (PAH, Zoion, Ardais, and AGF). All samples have been rendered anonymous, so investigators have no ability to identify the patients. Normal human tissues were obtained from patients undergoing routine surgery (multiple tissue, NDRI; stomach, Ardais Corporation; and colon, Cooperative Human Tissue Network), from short hour autopsy (≤ 5 h, multiple tissues; Zoion Diagnostics), and from transplant donors (lung, Anatomical Gift Foundation, Hanover, MD). All surgical samples were frozen as quickly as possible, typically within an hour of excision. The majority of samples were accompanied by demographic information and pathology reports.

Immunostaining of MDL-1. All human tissue experiments were performed in accordance with animal care and use committee–approved protocols. Immunohistochemistry was performed on frozen OCT embedded RA and OA synovia. 8-μm sections were fixed in acetone-methanol-hydrogen peroxide, and blocked with FCS-BSA-rat serum. Tissues were further blocked with avidin (Vector Laboratories) for 15 min and biotin (Vector Laboratories) for another 15 min. Sections were stained with anti–hMDL-1 mAb (clone DX245), anti-hCD68, or isotype control rat antibodies for 3 h and fixed with 1% paraformaldehyde. Tissues were washed and incubated with biotinylated rabbit anti–rat antibodies for 1 h, and Vectastain ABC elite horseradish peroxidase (HRP) complex for 40 min. Cell surface markers (MDL-1 and CD68) were visualized with Nova Red (Vector Laboratories) substrate and counterstained with methyl green.

Induction of CAIA and CIA. All animal experiments were performed in accordance with institutional animal care and use committe–approved protocols. Arthritis was induced in 8–16-wk-old (age-matched for a given study) male B10.RIII (Jackson ImmunoResearch Laboratories) with an arthritogenic anti-type II collagen mAb cocktail purchased from Chemicon International or Chondrex. B10RIII mice received 1–1.5 mg of anti-CII mAb cocktail i.v. on day 0. Mice were then treated s.c. with 0.5–1 mg of anti–MDL-1 or IgG1 isotype control. Alternatively, mice were treated s.c. with 0.5 mg of MDL-1 Ig-fusion protein or Ig-fusion control protein at day 0, 2, and 4. C57BL/6 mice received 5 mg arthrogen on day 0 and 10–50 μg of *E. coli*–derived LPS on day 2. Mice were monitored daily for foot pad swelling through day 11 or up to day 21.

12-16-wk-old B10RIII mice were immunized with 1 mg of bovine type-II collagen in a complete Freund's adjuvant (Difco) emulsion containing 2 mg/ml H37RA (Chondrex). Initial incidence of disease occurred at day 18 in 33–50% of all mice. On day 18, mice were given a single dose of 0.5 mg of anti–MDL-1 agonist or IgG1 isotype control. MDL-1 Ig-fusion protein (antagonist) or its corresponding mutant mouse Ig-fusion protein control were dosed every other day (starting on day 18) for a total of 6 doses. Mice were monitored for paw swelling through day 35. Paw swelling was measured daily after induction of arthritis. The severity of the disease was graded on a 0–3 scale per paw as follows: 0, normal; 1, swelling of one digit; 2, swelling of two or more digits; 3, swelling of the entire paw. The maximal clinical score per mouse was 12.

GR-1 depletion in antibody-induced arthritis (CAIA). 12-wk-old B10.RIII mice were dosed s.c. with 0.5 mg of anti-GR1 antibody (clone RB6-8C5) or IgG2b isotype control on day −1 before arthritis induction. Mice were given two subsequent s.c. doses of anti-GR1 or isotype on day 2 and 5 after disease induction.

Histopathological assessment. The paws were removed, fixed, decalcified in Cal-EX II (Thermo Fisher Scientific) for 7 d, and embedded in paraffin. Subsequently, the paw sections were stained with hematoxylin and eosin and examined by light microscopy. A histological analysis of synovial, bone, and cartilage tissues was performed as a blind test. Leukocyte infiltration and percentage of PMNs infiltration were determined in the synovium and joint space. Pannus tissue formation, cartilage destruction, and cortical bone erosions were assessed. The severity was graded on a scale of 0–4. Comparisons between groups were assessed with the two-tailed unpaired Student's *t* test with a P value of <0.05 considered as statistically significant. Calculations were performed with the statistical package, GraphPad Prism 4 (GraphPad Software, Inc.).

Histopathology scoring criteria is as follows. Inflammation in synovium and/or joint space: 0 = no inflammation, +1 = minimal, +2 = mild, +3 = moderate, +4 = severe; fibrosis (periarticular or pannus formation): +1 = minimal, +2 = mild, +3 = moderate, +4 = severe; percent PMNs: 1 = <20%, 2 = 20–40%, 3 = 40–60%, 4 = >60%; articular cartilage damage (destruction/pitting): +1 = minimal, +2 = mild, +3 = moderate, +4 = severe; cortical bone erosions/periosteal bone or cartilage proliferation: 0 = normal bone, +1 = minimal erosions, +2 = mild erosions, +3 = moderate, +4 = severe.

Macrophage and osteoclast culture assays. Macrophage cultures were generated from C57BL/6 or B10.RIII mice. Bone marrow was extracted from the femurs and tibias of 8–12-wk-old week animals. Cells were cultured for 1–5 d in basal macrophage growth medium, which is comprised of α-Mem media (Invitrogen), supplemented with 10% heat-inactivated fetal bovine serum, 100 IU/ml penicillin, 100 μg/ml streptomycin, 1 mM sodium pyruvate, 2 mM glutamine, and 50 ng/ml of recombinant MCSF (R&D Systems). Bone marrow–derived cells were cultured in various conditions and stained with biotinylated anti–MDL-1 (clone DX192). Samples were analyzed by FACSCalibur and FlowJo software (BD).

Osteoclasts were differentiated from bone marrow cells after 3 d culture in basal macrophage medium. Adherent cells were plated at $1–5 \times 10^5$ per ml in 6-well tissue culture plates and were treated with murine RANKL (10–50 ng/ml) and anti–MDL-1 or isotype control mAb at (10 μg/ml). Anti–MDL-1 activated cells were evaluated for osteoclast formation, gene expression, and TRAP staining (Acid phosphatase staining kit: Sigma) after 6–8 d in culture.

Nuclear NFATc1 quantification. NFATc1 is dephosphorylated upon activation by calcineurin in the cell cytoplasm and then translocated to the nucleus. To determine the ability agonist MDL-1 mAb to activate nuclear migration, 2×10^7 murine bone marrow cells were cultured in 10-mm dishes with 50 ng/ml of MCSF, 50 ng/ml of MCSF plus 30 ng/ml RANKL, and either 10 μg/ml of IgG1 isotype or anti–MDL-1 agonist antibody. Nuclear lysates were prepared from cells harvested at day 6 as described in Active Motif's nuclear extract kit. Nuclear samples were quantified by Bradford protein determination using lysis buffer as the diluent. 1-μg protein samples were run in duplicate on the NFATc1 assay. Plates were coated with an immobilized NFAT oligonucleotide consensus sequence (5′-AGGAAA-3′). The primary antibody specifically binds the accessible epitope on the NFATc1 protein. Secondary HRP-conjugated antibody allows colorimetric readout. Samples were visualized using SpectraMax (Molecular Devices) plate reader at 450 nm with a reference wavelength of 655. Samples were analyzed using SoftMax pro software (Molecular Devices), and nuclear

activation was assessed as compared with a titration PHA-activated Jurkat nuclear extract control.

Serum and tissue culture cytokine protein quantification. Blood samples were collected by cardiac puncture from euthanized mice. Serum was separated using serum separation tubes (Sarstedt) centrifuged at 6,000 *g*. Supernatants were collected from cell cultures and all samples were frozen at −80°C and thawed to room temperature before analysis. Protein and cytokine levels were analyzed by Luminex multiplex assays (LINCO Research). Murine serum TRAP 5b levels were ascertained by enzyme activity assay. (IDS, Inc.). Serum RANKL levels were determined by ELISA (R&D System).

Gene expression analysis. For gene expression analysis, total RNA was isolated using RNA STAT-60 (Tel-Test). Total RNA (5 μg) was subjected to treatment with DNase (Roche). DNase-treated total RNA was reverse-transcribed using Superscript II (Invitrogen). Primers were designed using Primer Express (PE Biosystems) or obtained commercially from Applied Biosystems. Real-time quantitative PCR on 10 ng of cDNA from each sample was performed using either of two methods. In the first method, two gene-specific unlabeled primers were used at 400 nM in a Perkin Elmer SYBR green real-time quantitative PCR assay using an ABI 5700 instrument. In the second method, two unlabeled primers at 900 nM each were used with 250 nM of FAM-labeled probe (Applied Biosystems) in a TAQMAN real-time quantitative PCR reaction on an ABI 7700 sequence detection system. The absence of genomic DNA contamination was confirmed using primers that recognize genomic regions of the CD4 promoter; samples with detectable DNA contamination by real-time PCR were excluded from the study. Ubiquitin levels were measured in a separate reaction and used to normalize the data by the $\Delta - \Delta$ Ct method, using the mean cycle threshold (Ct) value for ubiquitin and the genes of interest for each sample; the equation 1.8 e (Ct ubiquitin − Ct gene of interest) × 10^4 was used to obtain the normalized values.

Specimen preparation and imaging acquisition of three-dimensional microcomputed tomography. Mice were prepared for microCT analysis 14 d after CAIA disease induction. Hind paws were removed and fixed in 10% neutral buffered formalin. Before CT scanning, paws were washed with running water for 15 min. The imaging of three-dimensional microcomputed tomography was performed with GE eXplore Lotus micro-CT scanner (GE Healthcare). Data were acquired at 27 μm isotropic voxel size with 720 projections by 360-degree scan, integration time of 2,000 ms with three frames, photon energy of 80 KeV, and current of 450 uA. The duration of imaging time was ∼100 min per scan and followed by 1 h of projection correction and volume reconstruction of three-dimensional representation. Three-dimensional render images of hind paws were generated through original volumetric reconstructed images by MicroView software (GE Healthcare).

Bone histomorphometric measurements. The whole hind paw was scanned to quantify the histomorphometric measurements of the tarsal bones and of the metatarsal phalangeal joint. A three-dimensional region of interest (ROI) 3.2 × 2.0 × 1.8 mm^3 volume area was drawn to contain the second, third, and fourth metatarsal phalangeal joints. The profile of voxel densities changed dramatically in the mouse CAIA arthritic joint as inflammation-driven bone resorption gave rise to replacement of dense bone with less dense pannus tissue. The most high-density bone was lost in the metatarsal phalangeal joints of severely inflamed mouse CAIA paws. The greater proportion of "lower density bone" from 800–2,000 HU is caused by demineralization of a percentage of high-density bone within a voxel that gives rise to a lower density voxel after chronic inflammation. Four parameters were assessed to quantify the magnitude of bone loss: the total volume of bone (bone volume; BV), the total bone mineral content, represented by bone mass (bone mineral content; BM), and then the mean density of the bone (bone mineral density; BMD). BMD is the mass (BM) divided by the volume (BV). Total BV measurements in the metatarsal phalangeal joints encompass regions of trabecular and cortical bone. Mean cortical thickness analyses were performed using MicroView 2.2 software package to measure metatarsal phalangeal joint.

Peripheral blood analysis. Murine blood was harvested by cardiac puncture and collected in EDTA tubes (Terumo Medical Corp.) Blood samples were processed with Advia 120 Automated Hematology Analyzer. Percentage of monocytes, neutrophils, and high peroxidize positive (percentage of HPX) cells were compared with naive control mice.

Online supplemental material. Fig. S1 demonstrates a mast cell degranulation assay detecting the specific agonist activity of MDL-1. Fig. S2 shows micrographs of human RA synovial tissue stained for myeloid cell markers and MDL-1. Fig. S3 shows murine bone marrow and peripheral blood have increased numbers of MDL-1 positive cells after CAIA induction. Fig. S4 confirms depletion of a CD11b+ subset from blood after treatment with anti-GR1 antibody in CAIA. Fig. S5 shows collagen induced arthritis is exacerbated by agonist MDL-1 antibody treatment. Fig. S6 depicts the *Mdl1*$^{-/-}$ mouse gene targeting strategy. Fig. S7 shows the normalized gene expression values for WT, *Mdl1*$^{-/-}$, and *Dap12*$^{-/-}$ mice in CAIA model. Fig. S8 shows H&E staining from hind paws of mice in CAIA model where mice were treated with MDL-1 agonist and antagonist reagents. Online supplemental material is available at http://www.jem.org/cgi/content/full/jem.20090516/DC1.

We thank Dr. Craig A. Murphy for sharing his expertise in animal arthritis models. We thank Dr. Stuart Goodman for providing the RA synovial tissues. We also thank Drs. Mandy McGeachy and Cristina Tato for helpful discussion.

This study was funded by Schering-Plough Corporation.

The authors have no conflicting financial interests.

Submitted: 6 March 2009
Accepted: 20 January 2010

REFERENCES

Aoki, N., A. Zganiacz, P. Margetts, and Z. Xing. 2004. Differential regulation of DAP12 and molecules associated with DAP12 during host responses to mycobacterial infection. *Infect. Immun.* 72:2477–2483. doi:10.1128/IAI.72.5.2477-2483.2004

Bakker, A.B., E. Baker, G.R. Sutherland, J.H. Phillips, and L.L. Lanier. 1999. Myeloid DAP12-associating lectin (MDL)-1 is a cell surface receptor involved in the activation of myeloid cells. *Proc. Natl. Acad. Sci. USA.* 96:9792–9796. doi:10.1073/pnas.96.17.9792

Barck, K.H., W.P. Lee, L.J. Diehl, J. Ross, P. Gribling, Y. Zhang, K. Nguyen, N. van Bruggen, S. Hurst, and R.A. Carano. 2004. Quantification of cortical bone loss and repair for therapeutic evaluation in collagen-induced arthritis, by micro-computed tomography and automated image analysis. *Arthritis Rheum.* 50:3377–3386. doi:10.1002/art.20557

Chen, S.T., Y.L. Lin, M.T. Huang, M.F. Wu, S.C. Cheng, H.Y. Lei, C.K. Lee, T.W. Chiou, C.H. Wong, and S.L. Hsieh. 2008. CLEC5A is critical for dengue-virus-induced lethal disease. *Nature.* 453:672–676. doi:10.1038/nature07013

Henriksen, K., L.B. Tanko, P. Qvist, P.D. Delmas, C. Christiansen, and M.A. Karsdal. 2007. Assessment of osteoclast number and function: application in the development of new and improved treatment modalities for bone diseases. *Osteoporos. Int.* 18:681–685. doi:10.1007/s00198-006-0286-8

Humphrey, M.B., K. Ogasawara, W. Yao, S.C. Spusta, M.R. Daws, N.E. Lane, L.L. Lanier, and M.C. Nakamura. 2004. The signaling adapter protein DAP12 regulates multinucleation during osteoclast development. *J. Bone Miner. Res.* 19:224–234. doi:10.1359/JBMR.0301234

Humphrey, M.B., M.R. Daws, S.C. Spusta, E.C. Niemi, J.A. Torchia, L.L. Lanier, W.E. Seaman, and M.C. Nakamura. 2006. TREM2, a DAP12-associated receptor, regulates osteoclast differentiation and function. *J. Bone Miner. Res.* 21:237–245. doi:10.1359/JBMR.051016

Ishida, N., K. Hayashi, M. Hoshijima, T. Ogawa, S. Koga, Y. Miyatake, M. Kumegawa, T. Kimura, and T. Takeya. 2002. Large scale gene

expression analysis of osteoclastogenesis in vitro and elucidation of NFAT2 as a key regulator. *J. Biol. Chem.* 277:41147–41156. doi:10.1074/jbc.M205063200

Kaifu, T., J. Nakahara, M. Inui, K. Mishima, T. Momiyama, M. Kaji, A. Sugahara, H. Koito, A. Ujike-Asai, A. Nakamura, et al. 2003. Osteopetrosis and thalamic hypomyelinosis with synaptic degeneration in DAP12-deficient mice. *J. Clin. Invest.* 111:323–332.

Koga, T., M. Inui, K. Inoue, S. Kim, A. Suematsu, E. Kobayashi, T. Iwata, H. Ohnishi, T. Matozaki, T. Kodama, et al. 2004. Costimulatory signals mediated by the ITAM motif cooperate with RANKL for bone homeostasis. *Nature.* 428:758–763. doi:10.1038/nature02444

Lanier, L.L., B.C. Corliss, J. Wu, C. Leong, and J.H. Phillips. 1998. Immunoreceptor DAP12 bearing a tyrosine-based activation motif is involved in activating NK cells. *Nature.* 391:703–707. doi:10.1038/35642

Lee, S.H., J. Rho, D. Jeong, J.Y. Sul, T. Kim, N. Kim, J.S. Kang, T. Miyamoto, T. Suda, S.K. Lee, et al. 2006. v-ATPase V0 subunit d2-deficient mice exhibit impaired osteoclast fusion and increased bone formation. *Nat. Med.* 12:1403–1409. doi:10.1038/nm1514

Mao, D., H. Epple, B. Uthgenannt, D.V. Novack, and R. Faccio. 2006. PLCgamma2 regulates osteoclastogenesis via its interaction with ITAM proteins and GAB2. *J. Clin. Invest.* 116:2869–2879. doi:10.1172/JCI28775

Mathew, A., and A.L. Rothman. 2008. Understanding the contribution of cellular immunity to dengue disease pathogenesis. *Immunol. Rev.* 225:300–313. doi:10.1111/j.1600-065X.2008.00678.x

Matsumoto, M., M. Kogawa, S. Wada, H. Takayanagi, M. Tsujimoto, S. Katayama, K. Hisatake, and Y. Nogi. 2004. Essential role of p38 mitogen-activated protein kinase in cathepsin K gene expression during osteoclastogenesis through association of NFATc1 and PU.1. *J. Biol. Chem.* 279:45969–45979. doi:10.1074/jbc.M408795200

Mii, Y., Y. Miyauchi, T. Yoshikawa, K. Honoki, M. Aoki, M. Tsutsumi, H. Maruyama, M. Funauchi, Y. Konishi, and S. Tamai. 1991. Ultrastructural lipid and glycoconjugate cytochemistry of membranous lipodystrophy (Nasu-Hakola disease). *Virchows Arch. A Pathol. Anat. Histopathol.* 419:137–142. doi:10.1007/BF01600227

Ochi, S., M. Shinohara, K. Sato, H.J. Gober, T. Koga, T. Kodama, T. Takai, N. Miyasaka, and H. Takayanagi. 2007. Pathological role of osteoclast costimulation in arthritis-induced bone loss. *Proc. Natl. Acad. Sci. USA.* 104:11394–11399. doi:10.1073/pnas.0701971104

Paloneva, J., M. Kestilä, J. Wu, A. Salminen, T. Böhling, V. Ruotsalainen, P. Hakola, A.B. Bakker, J.H. Phillips, P. Pekkarinen, et al. 2000. Loss-of-function mutations in TYROBP (DAP12) result in a presenile dementia with bone cysts. *Nat. Genet.* 25:357–361. doi:10.1038/77153

Paloneva, J., T. Autti, R. Raininko, J. Partanen, O. Salonen, M. Puranen, P. Hakola, and M. Haltia. 2001. CNS manifestations of Nasu-Hakola disease: a frontal dementia with bone cysts. *Neurology.* 56:1552–1558.

Paloneva, J., J. Mandelin, A. Kiialainen, T. Bohling, J. Prudlo, P. Hakola, M. Haltia, Y.T. Konttinen, and L. Peltonen. 2003. DAP12/TREM2 deficiency results in impaired osteoclast differentiation and osteoporotic features. *J. Exp. Med.* 198:669–675. doi:10.1084/jem.20030027

Scarnecchia, L., S. Minisola, M.T. Pacitti, V. Carnevale, E. Romagnoli, R. Rosso, and G.F. Mazzuoli. 1991. Clinical usefulness of serum tartrate-resistant acid phosphatase activity determination to evaluate bone turnover. *Scand. J. Clin. Lab. Invest.* 51:517–524. doi:10.3109/00365519109104560

Takayanagi, H. 2005a. Mechanistic insight into osteoclast differentiation in osteoimmunology. *J. Mol. Med.* 83:170–179. doi:10.1007/s00109-004-0612-6

Takayanagi, H., S. Kim, T. Koga, H. Nishina, M. Isshiki, H. Yoshida, A. Saiura, M. Isobe, T. Yokochi, J. Inoue, et al. 2002. Induction and activation of the transcription factor NFATc1 (NFAT2) integrate RANKL signaling in terminal differentiation of osteoclasts. *Dev. Cell.* 3:889–901. doi:10.1016/S1534-5807(02)00369-6

Takayanagi, H., K. Sato, A. Takaoka, and T. Taniguchi. 2005b. Interplay between interferon and other cytokine systems in bone metabolism. *Immunol. Rev.* 208:181–193. doi:10.1111/j.0105-2896.2005.00337.x